Dynamic Gamma Modulation of Hippocampal Place Cells Predominates Development of Theta Sequences

Ning Wang[1], Yimeng Wang[1], Mingkun Guo[1], Ling Wang[1,2,3], Xueling Wang[1], Nan Zhu[1], Jiajia Yang[1,2,3], Lei Wang[4*], Chenguang Zheng[1,2,3,5*], Dong Ming[1,2,3]

1. Academy of Medical Engineering and Translational Medicine, Medical College, Tianjin University, Tianjin, China
2. Tianjin Key Laboratory of Brain Science and Neuroengineering, Tianjin, China
3. Haihe Laboratory of Brain-Computer Interaction and Human-Machine Integration, Tianjin, China
4. School of Statistics and Data Science, Nankai University, Tianjin, China
5. Lead contact

* Correspondence: L.W. (lwangstat@nankai.edu.cn) or C.Z. (cgzheng@tju.edu.cn)

ABSTRACT

The experience-dependent spatial cognitive process requires sequential organization of hippocampal neural activities by theta rhythm, which develops to represent highly compressed information for rapid learning. However, how the theta sequences were developed in a finer time scale within theta cycles remains unclear. In this study, we found that sweep-ahead structure of theta sequences developing with exploration was predominantly dependent on a relatively large proportion of FG-cells, i.e. a subset of place cells dominantly phase-locked to fast gamma rhythms. These ensembles integrated compressed spatial information entrained in a theta sequence by cells consistently firing at precessing slow gamma phases within the theta cycle. Accordingly, the sweep-ahead structure of FG-cell sequences was positively correlated with the intensity of slow gamma phase precession, in particular during early sequence development. These findings highlight the dynamic network-modulation by fast and slow gamma in the development of theta sequences which may further facilitate memory encoding and retrieval.

Keywords: Hippocampus, Place cells, Theta sequences, Gamma rhythms, Sequence development

INTRODUCTION

The hippocampus is known as its central role in encoding and storing experience and thus is essential for forming episodic memories (Buzsaki, McKenzie, & Davachi, 2022; Cohen & Eichenbaum, 1993). In the context of active navigation in an environment, hippocampal place cells are organized to fire sequentially within individual cycles of theta oscillations (4-12Hz) and form time-compressed representations of behavioral experiences, referred to as theta sequences (Colgin, 2020; Comrie, Frank, & Kay, 2022; Dragoi & Buzsaki, 2006; Skaggs, McNaughton, Wilson, & Barnes, 1996; Wallis, 2018). By sweeping ahead from the past to the upcoming locations, theta sequences represent information about potential future paths that could guide goal-directed behaviors (Gupta, van der Meer, Touretzky, & Redish, 2012; Joshi et al., 2023; Zheng, Hwaun, Loza, & Colgin, 2021). These predictive theta sequences exhibited experience-dependent development when rats were exploring a novel environment or learning a novel goal location (Feng, Silva, & Foster, 2015; Gobbo et al., 2022; Wikenheiser & Redish, 2015; Zheng et al., 2021). However, how the hippocampal network modulated the development of theta sequences' temporospatial-compressed organization remains incompletely understood.

A common assumption was established by previous studies that theta sequences were manifestations of theta phase precession, in which an individual place cell fired at progressively earlier theta phase as the animal traversed the place field (Aoki et al., 2023; Foster & Wilson, 2007; O'Keefe & Recce, 1993; Qasim, Fried, & Jacobs, 2021; Skaggs et al., 1996). However, when examined the theta sequences with experience at single trial level, their sequential structures were not developed on the first experience of a novel environment even if the phase

precession of individual place cells has been observed (Colgin, 2020; Feng et al., 2015). This suggests that the dynamic process of theta sequences development could be modulated by another network-level mechanism with neuronal firing organized at a finer timescale within theta cycles. Gamma (25-100Hz) could be a candidate that is thought to interact with theta to temporally organize theta sequences (Dragoi & Buzsaki, 2006; Fernandez-Ruiz, Sirota, Lopes-Dos-Santos, & Dupret, 2023; Lisman & Jensen, 2013). As two subtypes of gamma, fast and slow gamma rhythms (Colgin et al., 2009; Schomburg et al., 2014; Zhang, Lee, Rozell, & Singer, 2019) occur at distinct theta phases and coordinate theta sequences in different manners (Zheng, Bieri, Hsiao, & Colgin, 2016). This indicates that fast and slow gamma may act as different tuners but collaborate together in modulating theta sequence development.

Fast gamma (~65-100Hz), associated with the input from the medial entorhinal cortex, is thought to rapidly encode ongoing novel information in the context (Fernandez-Ruiz et al., 2021; Kemere, Carr, Karlsson, & Frank, 2013; Zheng et al., 2016). During fast gamma rhythms, place cell spikes occurred across all positions within a place field and displayed theta phase precession (Bieri, Bobbitt, & Colgin, 2014). This type of cells was identified recently as “phase-precessing” cells, in which the phase-precession pattern emerges with strong fast gamma (Guardamagna, Stella, & Battaglia, 2023). Their discrete distribution of theta phases is likely to contribute to the sequential structure formation when the sequences have been developed (Wang, Foster, & Pfeiffer, 2020). However, a question is raised about how these fast gamma-modulated cells be coordinated for the developmental process of theta sequences.

Slow gamma (~25-45Hz) in the hippocampal CA1 reflects information received

from CA3, which is responsible for the integration processing of learned information and experience (Colgin et al., 2009; Zhu et al., 2023). In contrast to fast gamma, spiking during slow gamma exhibited dominant theta phase locking and attenuated theta phase precession (Guardamagna et al., 2023; Zhang et al., 2019). This concentrated distribution of theta phase could be interpreted as they are coordinated within slow gamma cycles, as a finer time-scale than a theta cycle. Place cells spiking exhibited slow gamma phase precession, to generate mini-sequences in an individual theta sequence, for highly time-compressed representation of ongoing and future information (Zheng et al., 2016; Zheng et al., 2021). Thus, how fast and slow gamma rhythms coordinate place cells spiking to modulate the dynamic process of theta sequence development remains unclear.

Here, we proposed a scheme that fast gamma rhythms coordinate a subgroup of place cells for rapidly encoding and processing sensory information since from the early phase of theta sequence development (Fig.1). The developing process would be then dependent on the slow gamma modulation, that the spikes are fired at slow gamma phase-precessed pattern for spatial information compression within theta cycles. To test this hypothesis, we investigated how fast and slow gamma separately modulated place cells activities during the whole process of theta sequence development. We found that the fast gamma phase-locked place cells (FG-cells) were crucial for the development of theta sequences, without which the temporospatially compressed structure of theta sequences could not be developed. Furthermore, these cells exhibited slow gamma phase precession within theta cycles associated with the sweep-ahead structure of theta sequences, which occurred earlier than those cells not phase locked to fast gamma (NFG-cells). Our findings highlight the dynamic network-modulation by neural oscillations fast and slow

gamma, at finer timescales within theta, in development of theta sequences which may further facilitate memory encoding and retrieval.

RESULTS

A subgroup of hippocampal place cells phase locked to fast gamma rhythms during active behaviors

To investigate the temporal organization of place cells' firing associated with the gamma rhythms during the development of theta sequences, we recorded neuronal spiking of place cells and local field potentials simultaneously in hippocampal CA1 from 4 feely behaving rats (Fig.2-S1). As shown in a previous study, 32% of hippocampal pyramidal cells were phase-locked to gamma rhythms during waking theta states (Senior, Huxter, Allen, O'Neill, & Csicsvari, 2008). We further tested how the hippocampal place cells were modulated by slow and fast gamma rhythms respectively. The slow and gamma episodes were detected in time periods when the power of each gamma type (Fig.2A-B, fast gamma: 65-100 Hz, slow gamma: 25-45 Hz) was above a preset threshold (see Materials and Methods). We then detected the slow or fast gamma phase-locked place cells by quantifying the gamma phase distributions of all spikes across all trials. In this study, 488 place cells were included with place field distributed on the circular track but not located at the resting box. We found that 120 (24.6%) out of these cells were significantly phase-locked to gamma rhythms, a majority of which (113 cells, 23.2%) exhibited significant phase-locking to fast gamma rhythms (Fig.2C). Their preferred fast gamma phases (202.38±2.01 deg) were concentrated around the peak of fast gamma cycle, which was consistent with the findings in Schomburg et al. 2014 (Schomburg et al., 2014). However, a very small number (3.7%) of cells were found to phase-locked to slow gamma rhythms. Thus, these place cells were subdivided according to whether they were

134 significantly phase-locked to fast gamma (FG-cells) or not (NFG-cells) during active
135 behaviors in the subsequent analyses. Furthermore, the fast gamma phase-locking
136 of FG-cells was stable across trials, with a significantly higher mean vector length of
137 fast gamma phase-locking than those of NFG-cells (Fig.2D, repeated measure
138 ANOVA, main effect of cell type, $F(1,22)=33.9$, $p=7.5\times10^{-6}$, partial η^2 =0.6; main
139 effect of trials, $F(4,88)=1.3$, $p=0.3$, partial η^2 =0.06, no cell type x trials interaction,
140 $F(4,88)=0.5$, $p=0.8$, partial η^2 =0.02). Meanwhile, we also found that a larger
141 proportion of neurons in FG-cells had significant theta phase precession than NFG-
142 cell (Fig.2-S2, chi-squared test, ratio of theta phase precession cell among the FG-
143 cell vs. NFG-cell, n=457cell，$\chi^2=13.7$, $p=2.1\times10^{-4}$, Cramer V=0.2). These results
144 suggested that the FG-cells were stably modulated by fast gamma rhythms during
145 active behaviors.

146

147 **The FG-cells were crucial for theta sequence development**

148 As theta sequences were developed dependent on experience, we next
149 investigated whether FG-cells and NFG-cells played different roles in the
150 development of theta sequences. We then used a Bayesian decoding approach
151 (see Methods) to identify trajectories represented as rats running on a circular track,
152 and detected significant theta sequences in each single lap (Fig.3A). Another two
153 decoders were built by excluding either FG-cells spikes or down-sampled NFG-cells
154 spikes respectively, in order to compare the structures of theta sequences without
155 each type of cells. It can be observed that posterior probability distribution of theta
156 sequences was changed by excluding spikes from FG-cells (Fig.3B). The weighted
157 correlation of each sequence (Feng et al., 2015) was then measured to quantify the

temporospatial correlation of a theta sequence structure. We found that the weighted correlation of theta sequences decoded by excluding FG-cells spikes (exFG-sequences) was much lower than that of theta sequences decoded by excluding down-sampled NFG-cells spikes (exNFG-sequences) in the same theta cycles (Fig.3C, repeated measure ANOVA: main effect of cell type, $F(2,4844)=128.7$, $p=3.5\times10^{-48}$, partial $\eta^2=0.05$; post-hoc test, raw sequences vs. exFG-sequences, $p=8.0\times10^{-56}$, raw sequences vs. exNFG-sequences, $p=1.6\times10^{-26}$, exFG-sequences vs. exNFG-sequences, $p=4.1\times10^{-9}$). This suggests that the sequential structure could be dominantly interrupted by excluding FG-cells rather than NFG-cells.

Consistent with the previous studies (Feng et al., 2015; Wang et al., 2020), we also observed the development of theta sequences along with exploration experience (Fig.3D-E, repeated measure ANOVA, main effect of trials, $F(4,44)=7.0$, $p=2.0\times10^{-4}$, partial $\eta^2=0.4$). This could not be accounted for by running speed, as the rats were feely moving at stable running speed across trials (Fig.3F, repeated measure ANOVA, main effect of trials: $F(4,44)=0.9$, $p=0.5$ partial $\eta^2=0.07$). We further investigated whether the FG-cells or NFG-cells were required for the development of theta sequence structure. Interestingly, the temporospatial structure of the theta sequences cannot be developed with experience when the FG-cell spikes were excluded, with significantly lower weighted correlation than theta sequences constructed by excluding NFG-cell spikes (Fig.3D,G, repeated measure ANOVA, trials x cell type interaction, $F(4,44)=3.0$, $p=0.03$, partial $\eta^2=0.2$, main effect of cell type, $F(1,11)=7.8$, $p=0.02$, partial $\eta^2=0.4$; main effect of trials, $F(4,44)=4.0$, $p=0.008$). Since the theta sequences have been developed after Lap2, we defined the early development phase of sequences as the first 2 laps and late development phase of sequences as the last 2 laps of exploration experience, respectively. We

183 found that the weighted correlation of both exFG-sequences and exNFG-sequences
184 was low during early development (Fig.3H, paired t-test, t(24)=0.2, p=0.9, Cohen's
185 d=0.04). During late development, however, the weighted correlation of exNFG-
186 sequences was higher than that of exFG-sequences (Fig.3H, paired t-test, t(24)=-
187 3.7, p=0.001, Cohen's d=0.8). These results suggest that fast gamma modulation of
188 place cells may contribute to the development of theta sequence with exploration
189 experience.

190 In order to estimate to what extent, the FG cells contributed to theta sequence
191 development, we investigated the relationship between the percentage of FG-cells
192 and the formation of sequential structure in different developments. In our dataset,
193 the percentage of FG-cells out of all place cells varied across days, thus we detected
194 theta sequences from trials with relatively low percentage (~10%) and high
195 percentage (~35%) of FG-cells. The number of excluded NFG-cells for decoding
196 was matched up with the number of excluded FG-cells by a pseudo-random method
197 in each day. During early development, the temporospatial structure of theta
198 sequences has not been developed by excluding either low or high percentage of
199 each type of cells (Fig.4A). During late development, however, the sweeping-ahead
200 structure of the theta sequence was significantly disrupted when excluding a high
201 percentage (~35%) of FG-cells, which was not observed when excluding a low
202 percentage (~10%) of FG-cells (Fig.4B). The sequential structure could be
203 maintained by excluding NFG-cells at either low or high percentage. To quantify the
204 relationship between sequence structure and the number of excluded neurons during
205 early and late development, we then measured the weighted correlation difference
206 between exFG-sequences and exNFG-sequences as a function of the fraction of
207 excluded cells. The results showed that the weighted correlation difference was

close to 0 regardless of the fraction of excluded cells during early development (Fig.4C, Pearson's correlation, Corr=0.1, p=0.7). During late development, however, we found that the weighted correlation difference was positively correlated with the fraction of excluded cells (Fig.4D, Pearson's correlation, Corr=0.6, p=0.03). These results suggest different roles of FG-cells and NFG-cells in the development of the sweeping-ahead structure of theta sequence with experience, that the more temporospatially compressed structure of theta sequences may require a larger percentage of FG-cells.

In addition, we tested whether these results could be accounted for by the different firing characteristics between FG-cells and NFG-cells. We found that although these two types of cells took different proportion of all recorded place cells, the place fields of both types of cells could cover the entire track uniformly (Fig.2C, Fig.5A). We measured the distribution of center of mess (COM) of main place field of FG-cells and number-matched NFG-cells (Fig.5B), and found similar distribution of place field COM between cell types (Fig.5C, two-sample Kolmogorov-Smirnov test, Z=0.1, p=0.8). Furthermore, we found that the theta sequences in the above analyses were decoded by excluding similar numbers of spikes from FG-cells and NFG-cells (Fig.5D-E, Student’s t test, spike number: t(22)=1.8, p=0.09, Cohen’s D=0.7; mean firing rate in field: t(22)=2.0, p=0.06, Cohen’s D=0.8), indicating that the deferent development patterns between exFG-sequences and exNFG-sequences were not due to quality difference between two decoders. The two type of cells exhibited similar place fields size (Fig.5F, t(22)=0.7, p=0.5, Cohen’s D=0.3) and spatial information (Fig.5G, t(22)=1.0, p=0.3, Cohen’s D=0.4). These findings support the hypothesis that FG-cells, but not NFG-cells, may contribute to the development of theta sequences with experience.

233

234 **FG-cells exhibited slow gamma phase precession for information compression**
235 **required in theta sequence development**

236 In our previous study, we found that the place cell spikes occurred at
237 progressively earlier slow gamma phases across slow gamma cycles in theta
238 sequences, so-called slow gamma phase precession (Zheng et al., 2016). As
239 sequences of locations were represented at different slow gamma phases, theta
240 sequences exhibited temporospatially compressed structure representing long paths.
241 We next investigated if the development of theta sequence structure was related to
242 the slow gamma phase modulation of place cells. By detecting the slow gamma
243 phases of spikes within all theta cycles, we observed that the slow gamma phases
244 significantly shifted across successful slow gamma cycles (Fig.6A, multi-sample
245 Mardia-Watson-Wheeler test, $W(4)=369.4$, $p<2.2\times10^{-16}$; post-hoc test, Cycle -1 vs.
246 Cycle 0, $W(2)=97.5$, $p<2.2\times10^{-16}$, Cycle 0 vs. Cycle 1, $W(2)=95.4$, $p<2.2\times10^{-16}$),
247 which was consistent with the previous finding (Zheng et al., 2016). Then we
248 separated out the spike activity from the early and late development, and tested if
249 the slow gamma phase precession still existed during different developments.
250 Interestingly, we observed slow gamma phase shifting, but not phase precession,
251 across successive gamma cycles during early development. The distribution of slow
252 gamma phases in Cycle0 was similar as that in Cycle-1, then was dispersed in
253 Cycle1 (Fig.6B, multi-sample Mardia-Watson-Wheeler test, $W(4)=18.5$, $p=9.8\times10^{-4}$;
254 post-hoc test, Cycle -1 vs. Cycle 0, $W(2)=0.8$, $p=0.7$; Cycle 0 vs. Cycle 1, $W(2)=15.5$,
255 $p=4.4\times10^{-4}$). However, the slow gamma phase precession existed during late
256 development (Fig.6C, multi-sample Mardia-Watson-Wheeler test, $W(4)=21.2$,
257 $p=2.8\times10^{-4}$; post-hoc test, Cycle -1 vs Cycle 0, $W(2) = 8.8$, $p = 0.01$; Cycle 0 vs.

258 Cycle 1, W(2)=8.2, p=0.02). This finding suggests that slow gamma phase
259 precession of place cells may occur with exploring experience.

260 Furthermore, we investigated how the slow gamma phase precession occurred
261 in theta sequences developed with experience. We detected theta sequences
262 during slow gamma episodes and measured the distribution of phase shifts across
263 gamma cycles within single unites. In the significant theta sequences during slow
264 gamma episodes, we observed the slow gamma phase precession from single unit,
265 that the place cell spikes occurred at earlier slow gamma phases in later slow
266 gamma cycles (Fig.7A). To quantify the slow gamma phase precession at single unit
267 level, we calculated the phase shift as the phase difference within spike pairs from
268 adjacent active slow gamma cycles (See Methods). We found that slow gamma
269 phase difference was significantly lower than 0 between 2 active slow gamma cycles
270 (Fig.7B, one sample t-test, t(485)=-11.9, $p=6.3\times10^{-29}$, Cohen's D=0.5), as well as
271 among 3 or ≥4 active slow gamma cycles for strict limitation of theta sequences
272 modulated by slow gamma (3 active cycles, t(140)=-6.8, $p=3.0\times10^{-10}$, Cohen's
273 D=0.6; ≥4 active cycles, t(27)=-3.2, p=0.003, Cohen's D=0.6). Furthermore, we
274 averaged the slow gamma phase differences across different cells within a theta
275 sequence and compare their distribution along with learning trials. In the first lap, we
276 found that the slow gamma phase differences were not significantly different from
277 their surrogate data (Fig.7C, median of phase difference from lap1 was in 95%
278 confidence intervals of those from shuffled data, p=0.3). However, the distribution of
279 slow gamma phase difference was negatively biased compared with their surrogate
280 data (Fig.7C, median of phase difference from lap2-5 was beyond the 95%
281 confidence intervals of those from shuffled data; lap2 p=0.001, lap3 p=0.001, lap4
282 p=0.002, lap5 p=0.002). These results can also be replicated by averaging the slow

gamma phase differences from a single unit across succussive theta sequences (Fig.7D, lap1 p=0.1, lap2 p=0.001, lap3 p=0.001, lap4 p=0.002, lap5 p=0.01).

These findings raised a question of whether the development of slow gamma phase presession existed for both FG-cells and NFG-cells. To address this question, we quantified the distribution of slow gamma phase difference in FG-cells and NFG-cells respectively. We found that the slow gamma phase difference of FG-cells consistently exhibited a stable phase precession across trials, independent with learning experience (Fig.7E, lap1 p=0.007, lap2 p=0.006, lap3 p=0.007, lap4 p=0.002, lap5 p=0.02). In contrast, the slow gamma phase precession of NFG-cells was experience-dependent, with negative biased distribution of phase difference occurring from Lap2 (Fig.7E, lap1 p=0.9, lap2 p=0.01, lap3 p=0.001, lap4 p=0.009, lap5 p=0.1). These results suggest that FG-cells and NFG-cells have different dynamic modulated by slow gamma rhythms during exploration experience. The slow gamma modulation of FG-cells may occur earlier than that of NFG-cells, thereby driving the location information to be coded within theta cycles in a highly temporospatially compressed way.

FG-cells and NFG-cells exhibited different dynamics of slow gamma modulation along with theta sequence development

Finally, we wondered if there was correlation between slow gamma phase precession and the development of theta sequence structure, and how the FG-cells and NFG-cells coordinated during this process. Within each theta sequence, we measured its weighted correlation of the sequence structure, and plot it as a function of slow gamma phase difference across slow gamma cycles. Interestingly, we found

most data were distributed in the Quadrant1 (Q1) compared to the shuffled data distributed at the center (Fig.8A-B). The theta sequences with negative slow gamma phase difference and positive weighted correlation were significantly dominant (Fig.8C, the probability of observed data from lap1 exceeded 95% confidence intervals of those from shuffled data, p=0.001). This finding supports our hypothesis that the theta sequence development could be associated with the slow gamma phase precession.

We further investigated the contribution of FG-cells and NFG-cells to the slow gamma modulated theta sequence development during different exploring phases. Importantly, the distribution of FG-cell-dominant theta sequences was significantly biased to Q1 than that of the shuffled data, not only in late development when the theta sequences have been developed, but also in early development (Fig.8D-F, early development, p=0.001; late development, p=0.004). However, for NFG-cell-dominant theta sequences, their distribution was significantly biased to Q1 than that of the shuffled data only in late development (Fig.8G-I bottom, p=0.046), but not in early development (Fig.8G-I top, p=0.08). Taken together, these results support the hypothesis that FG-cells and NFG-cells may exhibit different dynamical characteristics in gamma modulation, thus their coordination may contribute to the development of theta sequences. FG-cells were consistently modulated by slow gamma phase precession, which would be precondition for theta sequence development.

DISCUSSION

In current study, we employed a circular track exploration task to investigate the

different roles of fast and slow gamma rhythms in the coordination of neurons during the experience-dependent development of theta sequences. We first found that a subgroup of place cells (FG-cells) that were phase-locked to fast gamma played a crucial role in the development of theta sequences. By excluding a sufficiently high proportion of FG-cells, the sweep-ahead structure of theta sequences was significantly disturbed compared to that of excluding equivalent number of NFG-cells. These FG-cells exhibited slow gamma phase precession within single theta cycles throughout the developing process of theta sequences. Finally, we showed positive correlation between the intensity of slow gamma phase precession and development of the sweep-ahead structure of theta sequences.

Fast gamma episodes were detected with dominantly high probability as initial exploration of each day and decreased probability as being familiar to the environment (Bieri et al., 2014). This could be related to the feedforward communication from upstream to downstream regions by using fast gamma frequencies (Vinck et al., 2023). Although the information propagation of visual stimulation was unlikely synchronized between visual cortex and hippocampal CA1 (Schneider, Tzanou, Uran, & Vinck, 2023), the MEC inputs could also be entrained by fast gamma to process ongoing sensory information to the hippocampus (Buzsaki & Schomburg, 2015; Colgin et al., 2009). Thus, the fast gamma phase-locked ensemble may act as a receiver of novel information that organized its intrinsic individual neurons in a time-compressed and spatially-ordered sequence to integrate the information under the mesoscopic cellular substrate modulated by fast gamma rhythms (Fernandez-Ruiz et al., 2023). These neurons exhibited similar firing characteristics as those of fast gamma non-phase-locked neurons, however, they showed higher probability presenting theta phase precession. Therefore, this fast

gamma phase-locked ensemble likely has overlapping with “bimodal cells” involved in the formation of theta sequence structure including reverse and forward windows (Chu et al., 2023; Wang et al., 2020). In this case, regardless of these neurons, the sweep-ahead structure of theta sequences could not be developed with learning, with the extent of structure impairment positively correlated with the proportion of excluded fast gamma phase-locked neurons.

The important role of fast gamma in modulating theta sequence development was also supported by a specific perturbation experiment. Liu and colleagues optogenetically entrained the MEC GABAergic cells at an artificial gamma frequency (53Hz) and observed the loss of phase precession patterns in CA1 place cells, and thereby the disrupted development of theta sequences (Liu, Todorova, Tang, Oliva, & Fernandez-Ruiz, 2023). The failure of sequential firing organization during behaviors impaired the formation of a predictive map related to the highly time-compressed awake replay sequences executing information storage. Fast gamma was also found diminished between MEC and CA1 in transgenic model mice of Alzheimer’s Disease, linked with spatial memory impairment in AD as a circuit mechanism(Jun et al., 2020). On the other hand, our previous study showed that fast gamma-dominated theta sequences represented shorter trajectories with relative less spatial information within a theta cycle (Zheng et al., 2016). This is indeed not contradictory with the current results, as we found that slow gamma, related to information compression, was also required to modulate fast gamma phase-locked cells during sequence development. We replicated the results of slow gamma phase precession at ensemble level (Zheng et al., 2016), and furthermore observed it at late development, but not early development, of theta sequences. Thus, a scenario could be drawn out that the network modulator was transitioned from fast gamma to

slow gamma throughout the sequence development with learning.

At single neuron level, we also observed that spikes of an individual place cell occurred at precessed slow gamma phases across consecutive slow gamma cycles under the time-scale of a theta window. At a finer scale within a theta cycle, slow gamma cycles coordinated place cells in a “mini-sequence” way (Zheng et al., 2016), in order to integrate information of long spatial trajectory related to the memory retrieval and predictive behaviors. This negatively-biased phase difference distribution appeared from lap2, when the sweep-ahead structures of theta sequences haven’t been fully developed, suggesting that slow gamma phase precession of place cells contributed to the information compression required to the theta sequence development. More interestingly, we found that slow gamma phase precession of a subset of neurons was absent at initial exploration when the theta phase precession has already displayed (Feng et al., 2015). This finding was in line with a previous study showing that silencing of CA3 output didn’t affect theta phase precession of a single cell, but impaired theta sequence structures (Middleton & McHugh, 2016). A possibility was that recruitment of PV-interneurons during the CA3-driven descending phase of the theta cycle, associated with the induction of slow gamma oscillations in CA1, was found reduced in the absence of CA3 input (Fernandez-Ruiz et al., 2023; Topolnik & Tamboli, 2022). We also provided additional evidence about the relationship between slow gamma phase precession and theta sequence formation, that the more negative slow gamma phase difference across cycles, the more sweep-ahead structure represented at late development of theta sequences.

It is noteworthy that the subset of neurons (FG-cells) was modulated by both fast gamma and slow gamma rhythms during the theta sequence development

(Fig.1). These place cells, associated with both memory encoding and retrieval, seem to function like memory engram-like representations (Goode, Tanaka, Sahay, & McHugh, 2020; Josselyn & Tonegawa, 2020; Lamothe-Molina et al., 2022; Pettit, Yap, Greenberg, & Harvey, 2022). Indeed, the proportion of c-Fos positive place cells (putative engram cells) had higher proportion being phase-locked to fast gamma than the c-Fos negative place cells (Tanaka et al., 2018). In contrast, the NFG-cells exhibited experience-dependent phase coding, that they likely contributed to the path representation at the late learning process. Thus, further studies would be needed to investigate how memory engram cells contribute to theta sequence development and facilitate spatial memory and navigation.

MATERALS AND METHODS

Subjects

Four male Long-Evans rats weighing 500 to 700g were used in this study. Rats were housed in custom-made acrylic cages (40cm×40cm×40cm) and exposed to a light cycle opposite to natural light (light exposure time: 8:00pm-8:00am). All waking activity recordings were performed in the dark (recording time: 8:00am-8:00pm). Rats were handled at the time of electrode implantation surgery and underwent at least 7 days of behavioral pretraining. Behavioral training was initiated after at least one week of recovery from implantation surgery. Rats were physically deprived during experimental data collection so that their body weight was maintained at ~90% of their free-feeding body weight. All experiments were conducted according to the guidelines of the Animal Care and Use Committee of Tianjin University.

Behavioral paradigm

We designed a circular track apparatus for this study. The circular track with an inner diameter of 90 cm, height of 50 cm, and width of 10 cm, was placing an acrylic resting box (height of 31 cm, length of 28 cm, and width of 21cm) as beginning and ending. Each rat underwent training to navigate on a circular track. A total of eighteen small black silicone dots were utilized as context cues along the circular track, covering approximately two-thirds of its length. Each dot was at a distance of 12 cm (or equivalently 0.28 radians) away from its neighbors. Before surgery, all rats were pre-trained on the same circular track for 1 week and recovered from surgery for at least one week before behavioral training resumed. For every recording session, rats ran 5 trials (or laps) on the circular track. For each running lap, the rats started from the rest box, navigating clockwise to the rest box, and then returned to the rest box counter-clockwise without receiving any food reward. A tone (1kHz sine wave with a duration of 0.25s) was delivered at the beginning and end of the trial. According to the recorded position, the 2D movement speed of the rat was calculated by 2D coordinates and elapsed times of consecutive two points.

Surgery and tetrode implanting

Before surgery, tetrodes were built from 17μm polyimide-coated platinum-iridium (10/90%) wire (California Fine Wire, Grover Beach, California). The tetrode tip was platinum-plated using a NanoZ system (White Matter, Seattle, Washington), ensuring that the impedance of each recording channel was below 300 kOhms to facilitate single-neuron activity recording. Eighteen independently mobile tetrodes hyperdrive were surgically implanted into the hippocampal dorsal CA1 region. The rat brain stereotaxic coordinates of the center of the electrode bundle were anterior-posterior [AP] -3.5 mm, medial-lateral [ML] 3.0mm and on day of implantation the tetrode tips moved 1mm downward (dorsal-ventral [DV] 1mm). Screws were placed on the

surface of the skull. The hyperdrive bundle were attached to the screws and skull with dental cement. Two screws placed in the skull above the cerebellum served as a panel ground for recording. After surgery, tetrodes were gradually downward to dCA1 stratum pyramidale. One tetrode was designed as recording reference. Recording reference was used to differentiate from other recording tetrode to monitor signal During other recording tetrode downwards, the recording reference was moved up and down to a quiet position in the cortex above the hippocampus and remained quiet throughout signal recording session.

Data acquisition

Behavioral and electrophysiological data were acquired using a Digital Lynx system and Cheetah recording software (Neuralynx, Bozeman, Montana). LFPs recorded continuously from a single channel in each tetrode, within the frequency range of 0.1-500 Hz from raw signal at 2,000 Hz sampling rate. Before each recording session starting, the input amplitude ranges were carefully adjusted to optimize resolution and prevent signal saturation. Typically, the input ranges for LFPs were within the range of ±2,000 μV to 3000μV. To detect unit activity, signals from each channel in a tetrode were bandpass filtered from 600 to 6,000 Hz. The spike detected threshold was 55 μV. All the recorded signals were obtained by differentiating with the reference tetrode (see “surgery and tetrode planting”), eliminating a large amount of background noise. The position of the rat during navigation behavior was recorded by the video tracking function within Neuralynx system. The video resolution of 720 × 480 pixels and a frame rate of 25 frames per second. The actual position was tracked with a red light-emitting-diode (LED) on one of the three HS-27-Mini-LED headstage (Neuralynx, Bozeman, Montana) attached to the hyperdrive. The actual 2D coordinates were obtained according to

the pixel value where the red is brightest

Spike sorting

Detected spikes were manually sorted using graphical cluster-cutting software (MClust; A.D. Redish, University of Minnesota, Minneapolis). Spikes were sorted using two-dimensional projections of three different features of spike waveforms (i.e., energies, peaks, and peak-to-valley differences) from four channels. Clusters were judged based on waveform shape, isolation distance, and lack of inter-spike-interval violation. Units with mean firing rates of more than 15 Hz were identified as putative fast-spiking interneurons and were excluded from further analysis. The units with peak firing rates more than 1 Hz but mean firing rates of less than 15 Hz was putative pyramidal cell for further analysis.

Spatial firing maps and place cell identification

The animal position on the circular track was linearized to increasing radian values and divided into 90 bins (approximately 0.035 rad per bin and that is 3.5cm). Spatial firing maps were calculated only during locomotor periods (> 5cm/s). To calculate directional spatial firing rate-maps, the number of directional spikes was divided by the time of occupancy at each position bin on the circular track with the same direction, followed by smoothing with a Gaussian kernel (standard deviation of 2 bins). For identifying the place cell, we used all trial spikes to calculate rate-maps. A continuous span of at least three consecutive bins in the rate-map with a peak firing rate exceeding 1 Hz was calculated as a place field. A pyramidal cell contained at least one place field was defined as a place cell. The place field size was defined by 0.1Hz firing rate boundary. The firing rate in each place field is divided by the number of bins in the field to calculate the mean firing rate in the field, the peak firing rate. The primary place field used for analysis was defined as the field with the

maximal peak firing rate among all fields. Finally we accepted 488 place cells with place field distributed on the circular track (region from dot 1 to 18) but not located at the resting box.

Spatial specificity was quantified by computing the spatial information score (Langston, Ainge et al. 2010). For each cell, the spatial information score in bits per spike was calculated from the recording in each period as:

$$\text{Spatial information} = \sum_i P_i \frac{\lambda_i}{\lambda} \log_2 \frac{\lambda_i}{\lambda}$$

Where λ_i is the mean firing rate of a unit the ith bin, λ is the overall mean firing rate, and p_i is the probability of the animal being in the ith bin (occupancy in the ith bin/total occupancies bin).

The single-lap(or trial) rate-maps was calculated using the same method and used to Bayesian decoding analysis.

Local field potential analysis

Theta, slow gamma, and fast gamma rhythms were extracted from the LFP by applying band-pass filters with frequency ranges of 4-12 Hz, 25-45 Hz, and 65-100 Hz, respectively. The time-varying phases of the theta, slow gamma, and fast gamma rhythms were computed using the Hilbert transform. As the previous study showed, the gamma power spectra were measured across different running speeds. The power spectra across running speeds and absolute power spectrum (both result were not shown) was estimated through the multitaper spectral analysis (Mitra and Bokil, 2008) in the Chronux toolbox (http://chronux.org/). We defined the gamma episode as the 160ms window with gamma power higher than 3 standard deviations to observe the firing activity of place cells.

Quantification of theta phase precession

Theta phase precessions were examined in the primary place field calculated by all trial spikes. The phase-position correlation of spikes emitted by a place cell during all lap of its place field was determined by circular-linear regression between the theta phase of spikes and the actual position of animal. The significant negative correlation was determined theta phase precession. Theta phase precession slope was calculated by least-square fit of spike locations of the animal and shifted spike phases.

Estimation of gamma phase-locking

Phase-lock analysis was implemented using custom scripts based on the circ_stats function from Matlab CircStat toolbox. The slow gamma, and fast gamma spike phase distributions for each place cell were then determined by the time-varying phases of slow gamma, and fast gamma (see “Local field potential analysis”), respectively, at the time point closest to each spike time. And each spike phase was evaluated with the LFP recorded in the tetrode where the neuron was located. Phase-locking was quantified by calculating the mean vector length of the resulting phase distributions. Significant phase-locking at fast gamma is identified only for place cells meeting the criteria of a Rayleigh test $p<0.05$ and firing at least 10 spikes on each lap. For easy presentation, these cells are named FG-cells. The remaining place cell are not phase-locking at fast gamma, called NFG-cells. According to our results, nearly a quarter of the neurons are significantly phase-locked at fast gamma. Only a very small number of neurons are slow gamma phase-locked.

Single-trial Bayesian decoding analysis

To translate ensemble spiking activity into radian positions on the circular track, a memory-less Bayesian decoding algorithm was implemented. Decoding was

performed using a 20ms sliding time window that shifted 5ms at each step. For each decoding window, the number of spikes occurring is denoted as n_i, so that the vector of all spiking activity simultaneously recorded for the cell is $\boldsymbol{n} = \{n_1, n_2, \cdots, n_i\}$. The probability of a rat being at position x, given the number of spikes $\boldsymbol{n}$ from each unit recorded in a time window, was estimated by Bayes' rule:

$$P(x|\boldsymbol{n}) = \frac{P(\boldsymbol{n}|x) \times P(x)}{P(n)}$$

where $P(\boldsymbol{n}|x)$ was approximated from the single directional firing turning curve of each unit. The approximation assumed that the turning curve of individual units was statistically independent and the number of spikes from each unit followed a Poisson distribution. Prior knowledge of position $P(x)$ was set to 1 to avoid decoding bias to any particular location on the track. The normalizing constant $P(n)$ was set to ensure $P(x|\boldsymbol{n})$, or posterior probability, summed to 1. The decoding position was is the set of x that maximizes $P(x|\boldsymbol{n})$. Decoding error was defined as the distance between the decoded position with maximum-likelihood and the rat's true position. For excluded cell decoding, position reconstruction was performed by removing the FG-cells or NFG-cells from $\boldsymbol{n}$, respectively. Bayesian decoding analyses were performed using custom routines in MATLAB 2020b.

Theta cycle detection

A single tetrode located in the stratum pyramidale and physical center all recording tetrodes was selected and the theta signal (including phase and power etc.) from this tetrode was utilized for further analysis. According to previous studies, almost all theta sequences fall completely into a theta cycle. Therefore, the global 0 phase (the beginning of the theta cycle) of theta rhythm was determined as the phase when the theta sequence quantization indicators (see "Theta sequence

576 quantification”) were maximal. Briefly, the global 0 phase was moved from the peaks
577 in steps of 10°, and in every step, the sequence of place cells was quantified in each
578 theta cycle. The peak of the histogram of the distribution of the quantization
579 indicators over the step size was used as the global 0 theta phase for further
580 analysis.

581 **Theta sequence quantification**

582 Theta sequences were quantified only when the following conditions also hold:
583 (1) the animal was in the middle of the track (two-thirds of the circular track length),
584 (2) the current running direction is consistent with the expected direction with running
585 faster than 5 cm/s, (3) the duration of the corresponding theta cycles ranged from
586 100 to 200 ms, (4) more than 3 place cells and emitted at least 5 spikes during the
587 corresponding theta cycle.

588 Averaged sequence was constructed over the laps by aligning the probabilities
589 over the theta cycle mid-time point and position. Each and averaged sequence were
590 quantified within an area that decoded probabilities ±35 cm around the position of
591 animal, and ±1⁄4 theta cycle around the mid-time point of the theta sequence.

592 ***Probability difference***

593 The area used to quantify were divided equally into four quadrants. The
594 Quadrant 2 represents the region both physically and temporally ahead of the rat,
595 whereas as the Quadrant 3 represents the region physically and temporally behind
596 the rat. Quadrant 1 and 4 represents the region that opposite with the animal’s
597 current running direction. The summed decoded probabilities in Quadrant 1 and 4
598 were subtracted from the summed decoded probabilities in Quadrant 2 and 3 then
599 divided by the summed decoded probabilities in all four quadrants. This value
600 represents the difference between the decoding probability of the normalized current

path and the opposite path in the theta sequence. Positive differences would imply theta sequences sweeping ahead in current moving direction of the rat, whereas differences close to zero would indicate a lack of sequential structure.

Weighted correlation

Weighted correlation of each or averaged theta sequence was calculated from the same area mentioned above. With the decoding probability (*prob*) as the weight of the position estimation, the correlation coefficient between the time (*t*) and the decoding position (*p*) is as follows:

$$corr_w(t,p;prob) = \frac{cov(t,p;prob)}{\sqrt{cov(t,t;prob)cov(p,p;prob)}}$$

where weighted covariance between time and decoded position is as follows:

$$cov(t,p;prob) = \frac{\sum_i prob_i(t_i - m(t;prob))(p_i - m(p;prob))}{\sum_i prob_i}$$

and weighted means of time and decoded position are as follows:

$$m(t;prob) = \frac{\sum_i prob_i\, t_i}{\sum_i prob_i}$$

and

$$m(p;prob) = \frac{\sum_i prob_i\, p_i}{\sum_i prob_i}$$

The apparent sweep-ahead structure in the current running direction of animal produced large positive correlations (close to one), whereas the lack of sequence structure produced close to zero correlations. For further analysis, we use weighted correlation to quantify the theta sequence from different decoding result.

Flip correlation difference

We defined an Indicator to measure the front-sweep structure, named Flip correlation difference, which of each or averaged theta sequence was calculated

also from the same area mentioned above. In the temporal dimension, the correlation coefficient between the decoding probability and the decoding probability after performing both temporal and spatial flips was calculated, from which the correlation coefficient between the decoding probability and the decoding probability after performing only temporal flips was subtracted. Positive difference represents intact sequential structure in the positive, whereas differences close to zero or negative would indicate a lack of sequential structure or defective sequential structure.

Gamma phase shift analysis of cell ensemble

The gamma cycle with maximal spiking across all simultaneously recorded cells was defined as cycle 0. Gamma cycles occurring before cycle 0 are represented by decreasing integer values, after by increasing integer values. Incomplete cycles at the beginning or end of the sequence or during immobile (speed<5cm/s) were excluded from analyses. We estimated the gamma phases and theta phases of spike times for place cells that exhibited spikes within at least two slow gamma cycles or at least three fast gamma cycles within a single theta cycle. The number of cycles analyzed within each theta sequence was limited to three (cycles -1 to 1) for slow gamma and five (cycles -2 to 2) for fast gamma (data not shown). Two-dimensional histograms of gamma phases and theta phases for spikes from each cycle number were binned into 40 bins and smoothed across nine bins.

Slow gamma phase shift analysis of individual cell

We employed Morlet's wavelet method to calculate the time-varying power of slow gamma. The slow gamma energy in each theta cycle was estimated, considering only cycles with energy higher than 1.5 times the standard deviation as slow gamma events. The global 0 phase of slow gamma, set at the trough,

determined the phase shift. For each cell, spikes in different slow gamma cycles within each theta cycle were identified. Spike pairs, representing adjacent spikes from different slow gamma cycles, were used to calculate the average phase difference as the slow gamma phase difference. In cases of multiple spikes in the same slow gamma cycle, their average phase was taken. Negative values indicated phase precession, while positive values indicated procession. To maintain firing location constancy, spikes used for phase difference calculation were assigned a random slow gamma phase within their cycle, repeated 1000 times for a distribution. In the analysis, we calculated one-sided, corrected empirical p-values [(r+1)/(n+1)] by comparing real data to its corresponding shuffle data. Where r is the number values from the shuffled distribution that are either smaller or larger (depending on the hypothesis) than the observed value and n=1000 is the number of shuffling.

Correlation between the slow gamma phase precession and weighted correlation

The theta cycle satisfying the criteria (see Slow gamma phase shift analysis) for calculating the phase difference was chosen to estimate the relationship between slow gamma phase precession and weighted correlation. On the one hand, the Pearson correlation coefficient was used to estimate the linear correlation between them. On the other hand, the correlation between slow gamma phase precession and theta sequence structure was analyzed by two-dimensional histogram. We binned slow gamma phase difference and weighted correlation into ten bins to construct a two-dimensional histogram, and smoothed it across three bins for visualize. The Two-dimensional histogram was divided into four quadrants and the sum of probability in Quadrant 1 (Q1) was calculated. The statistical significance was determined by calculating the one-sided, corrected empirical p-value. The

shuffle data was same as slow gamma phase shuffle. The true data was considered to be significantly concentrated in Q1. The null hypothesis was the probability in Q1 of shuffled data was larger than the true data. If the p value was less than 0.05, the null hypothesis was rejected.

Histology

At the end of the experiment, histological sections were prepared as follows to verify the tetrodes position. Rats were intraperitoneally injected with a lethal dose of urethane solution. The heart was subsequently perfused with phosphate buffer and formalin to fix the brain tissue. Rat brains were then cut into 30-μm coronal sections and Nissl Staining was performed to determine the location of tetrode in CA1.

Quantification and statistical analysis

Data analyses were performed using SPSS (IBM) and custom Matlab (the Math Work) and R scripts. Paired t-test was performed to test between exFG-sequences and exNFG-sequences during early and late development (Fig.3H). Student's t test was performed to test the spike number, mean firing rate in field, place fields size and spatial information between the FG-cell and NFG-cell (Fig.5D-G). One-sample t test was conducted to assess whether the slow gamma phase shift was significantly lower than 0 (Fig.7B). Repeated measures ANOVA was performed to test the weighted correlation of theta sequences (Fig.2D, Fig.3C,E,G) and running speed (Fig.3F) as a function of laps. Kolmogorov-Smirnov test was performed to test the distribution of place field COM (Fig.5C) on the track using the Matlab function 'kstest2'. Multi-sample Mardia-Watson-Wheeler test was performed to test the slow gamma phase shift of place cells across successive slow gamma cycles (Fig.6) using the R 'circular-package'. Pearson's correlation was performed to test the correlation between weighted correlation difference and the proportion of excluded

cells (Fig.4C-D).

ACKNOWLEDGMENTS

We thank Shuang Meng for help with rat behavioral pre-training; and all Zheng Lab members for helpful discussions. This work was supported by the grants from National Science and Technology Innovation 2030 Major Project of China (2022ZD0205000), National Natural Science Foundation of China (T2322021, 82271218 to C.Z., 12271272 to L.W., 81925020 to D.M., 82371886 to J.Y., 82202797 to L.W.), The Space Brain Project from Lingang Laboratory (LG-TKN-202204-01 to J.Y.), and the China Post-Doctoral Science Foundation (2022M712365 to L.W.).

AUTHOR CONTRIBUTIONS

Conceptualization, C.Z. and L.W.; Methodology and Software, N.W., L.W. and C.Z.; Investigation, N.W., Y.W., M.G., L.W. N.Z., X.W. and C.Z.; Formal Analysis, N.W. and L.W.; Writing – Original Draft, N.W. and C.Z.; Funding Acquisition, C.Z., M.D., L.W., J.Y., and L.W.; Supervision, C.Z. and D.M.

COMPETING INTERSETS

The authors declare that they have no competing interests.

REFERENCES

Aoki, Y., Yokoi, T., Morikawa, S., Kuga, N., Ikegaya, Y., & Sasaki, T. (2023). Effects of theta phase precessing optogenetic intervention on hippocampal neuronal reactivation and spatial maps. *iScience, 26*(7), 107233. doi:10.1016/j.isci.2023.107233

Bieri, K. W., Bobbitt, K. N., & Colgin, L. L. (2014). Slow and fast gamma rhythms coordinate different spatial

coding modes in hippocampal place cells. *Neuron, 82*(3), 670-681. doi:10.1016/j.neuron.2014.03.013

Buzsaki, G., McKenzie, S., & Davachi, L. (2022). Neurophysiology of Remembering. *Annual Review of Psychology, 73*, 187-215. doi:10.1146/annurev-psych-021721-110002

Buzsaki, G., & Schomburg, E. W. (2015). What does gamma coherence tell us about inter-regional neural communication? *Nature Neuroscience, 18*(4), 484-489. doi:10.1038/nn.3952

Chu, T., Ji, Z., Zuo, J., Mi, Y., Zhang, W., Huang, T., . . . Wu, S. (2023). Firing rate adaptation affords place cell theta sweeps, phase precession and procession. *Elife, 12*, RP87055.

Cohen, N. J., & Eichenbaum, H. (1993). *Memory, amnesia, and the hippocampal system*. Cambridge, MA, US: The MIT Press.

Colgin, L. L. (2020). Five Decades of Hippocampal Place Cells and EEG Rhythms in Behaving Rats. *J Neurosci, 40*(1), 54-60. doi:10.1523/JNEUROSCI.0741-19.2019

Colgin, L. L., Denninger, T., Fyhn, M., Hafting, T., Bonnevie, T., Jensen, O., . . . Moser, E. I. (2009). Frequency of gamma oscillations routes flow of information in the hippocampus. *Nature, 462*(7271), 353-357. doi:10.1038/nature08573

Comrie, A. E., Frank, L. M., & Kay, K. (2022). Imagination as a fundamental function of the hippocampus. *Philos Trans R Soc Lond B Biol Sci, 377*(1866), 20210336. doi:10.1098/rstb.2021.0336

Dragoi, G., & Buzsaki, G. (2006). Temporal encoding of place sequences by hippocampal cell assemblies. *Neuron, 50*(1), 145-157. doi:10.1016/j.neuron.2006.02.023

Feng, T., Silva, D., & Foster, D. J. (2015). Dissociation between the experience-dependent development of hippocampal theta sequences and single-trial phase precession. *Journal of Neuroscience, 35*(12), 4890-4902. doi:10.1523/JNEUROSCI.2614-14.2015

Fernandez-Ruiz, A., Oliva, A., Soula, M., Rocha-Almeida, F., Nagy, G. A., Martin-Vazquez, G., & Buzsaki, G. (2021). Gamma rhythm communication between entorhinal cortex and dentate gyrus neuronal assemblies. *Science, 372*(6537). doi:10.1126/science.abf3119

Fernandez-Ruiz, A., Sirota, A., Lopes-Dos-Santos, V., & Dupret, D. (2023). Over and above frequency: Gamma oscillations as units of neural circuit operations. *Neuron, 111*(7), 936-953. doi:10.1016/j.neuron.2023.02.026

Foster, D. J., & Wilson, M. A. (2007). Hippocampal theta sequences. *Hippocampus, 17*(11), 1093-1099. doi:10.1002/hipo.20345

Gobbo, F., Mitchell-Heggs, R., Tse, D., Al Omrani, M., Spooner, P. A., Schultz, S. R., & Morris, R. G. M. (2022). Neuronal signature of spatial decision-making during navigation by freely moving rats by using calcium imaging. *Proc Natl Acad Sci U S A, 119*(44), e2212152119. doi:10.1073/pnas.2212152119

Goode, T. D., Tanaka, K. Z., Sahay, A., & McHugh, T. J. (2020). An Integrated Index: Engrams, Place Cells, and Hippocampal Memory. *Neuron, 107*(5), 805-820. doi:10.1016/j.neuron.2020.07.011

Guardamagna, M., Stella, F., & Battaglia, F. P. (2023). Heterogeneity of network and coding states in mouse CA1 place cells. *Cell Reports, 42*(2), 112022. doi:10.1016/j.celrep.2023.112022

Gupta, A. S., van der Meer, M. A., Touretzky, D. S., & Redish, A. D. (2012). Segmentation of spatial experience by hippocampal theta sequences. *Nature Neuroscience, 15*(7), 1032-1039. doi:10.1038/nn.3138

Joshi, A., Denovellis, E. L., Mankili, A., Meneksedag, Y., Davidson, T. J., Gillespie, A. K., . . . Frank, L. M. (2023). Dynamic synchronization between hippocampal representations and stepping. *Nature, 617*(7959), 125-131. doi:10.1038/s41586-023-05928-6

Josselyn, S. A., & Tonegawa, S. (2020). Memory engrams: Recalling the past and imagining the future. *Science, 367*(6473), eaaw4325. doi:10.1126/science.aaw4325

Jun, H., Bramian, A., Soma, S., Saito, T., Saido, T. C., & Igarashi, K. M. (2020). Disrupted Place Cell

Remapping and Impaired Grid Cells in a Knockin Model of Alzheimer's Disease. *Neuron, 107*(6), 1095-1112 e1096. doi:10.1016/j.neuron.2020.06.023

Kemere, C., Carr, M. F., Karlsson, M. P., & Frank, L. M. (2013). Rapid and continuous modulation of hippocampal network state during exploration of new places. *PLoS One, 8*(9), e73114. doi:10.1371/journal.pone.0073114

Lamothe-Molina, P. J., Franzelin, A., Beck, L., Li, D., Auksutat, L., Fieblinger, T., . . . Oertner, T. G. (2022). DeltaFosB accumulation in hippocampal granule cells drives cFos pattern separation during spatial learning. *Nat Commun, 13*(1), 6376. doi:10.1038/s41467-022-33947-w

Lisman, J. E., & Jensen, O. (2013). The theta-gamma neural code. *Neuron, 77*(6), 1002-1016. doi:10.1016/j.neuron.2013.03.007

Liu, C., Todorova, R., Tang, W., Oliva, A., & Fernandez-Ruiz, A. (2023). Associative and predictive hippocampal codes support memory-guided behaviors. *Science, 382*(6668), eadi8237. doi:10.1126/science.adi8237

Middleton, S. J., & McHugh, T. J. (2016). Silencing CA3 disrupts temporal coding in the CA1 ensemble. *Nature Neuroscience, 19*(7), 945-951. doi:10.1038/nn.4311

O'Keefe, J., & Recce, M. L. (1993). Phase relationship between hippocampal place units and the EEG theta rhythm. *Hippocampus, 3*(3), 317-330. doi:10.1002/hipo.450030307

Pettit, N. L., Yap, E. L., Greenberg, M. E., & Harvey, C. D. (2022). Fos ensembles encode and shape stable spatial maps in the hippocampus. *Nature, 609*(7926), 327-334. doi:10.1038/s41586-022-05113-1

Qasim, S. E., Fried, I., & Jacobs, J. (2021). Phase precession in the human hippocampus and entorhinal cortex. *Cell, 184*(12), 3242-3255 e3210. doi:10.1016/j.cell.2021.04.017

Schneider, M., Tzanou, A., Uran, C., & Vinck, M. (2023). Cell-type-specific propagation of visual flicker. *Cell Rep, 42*(5), 112492. doi:10.1016/j.celrep.2023.112492

Schomburg, E. W., Fernandez-Ruiz, A., Mizuseki, K., Berenyi, A., Anastassiou, C. A., Koch, C., & Buzsaki, G. (2014). Theta phase segregation of input-specific gamma patterns in entorhinal-hippocampal networks. *Neuron, 84*(2), 470-485. doi:10.1016/j.neuron.2014.08.051

Senior, T. J., Huxter, J. R., Allen, K., O'Neill, J., & Csicsvari, J. (2008). Gamma oscillatory firing reveals distinct populations of pyramidal cells in the CA1 region of the hippocampus. *Journal of Neuroscience, 28*(9), 2274-2286. doi:10.1523/JNEUROSCI.4669-07.2008

Skaggs, W. E., McNaughton, B. L., Wilson, M. A., & Barnes, C. A. (1996). Theta phase precession in hippocampal neuronal populations and the compression of temporal sequences. *Hippocampus, 6*(2), 149-172. doi:10.1002/(SICI)1098-1063(1996)6:2<149::AID-HIPO6>3.0.CO;2-K

Tanaka, K. Z., He, H., Tomar, A., Niisato, K., Huang, A. J. Y., & McHugh, T. J. (2018). The hippocampal engram maps experience but not place. *Science, 361*(6400), 392-397. doi:10.1126/science.aat5397

Topolnik, L., & Tamboli, S. (2022). The role of inhibitory circuits in hippocampal memory processing. *Nat Rev Neurosci, 23*(8), 476-492. doi:10.1038/s41583-022-00599-0

Vinck, M., Uran, C., Spyropoulos, G., Onorato, I., Broggini, A. C., Schneider, M., & Canales-Johnson, A. (2023). Principles of large-scale neural interactions. *Neuron, 111*(7), 987-1002. doi:10.1016/j.neuron.2023.03.015

Wallis, J. D. (2018). Decoding Cognitive Processes from Neural Ensembles. *Trends Cogn Sci, 22*(12), 1091-1102. doi:10.1016/j.tics.2018.09.002

Wang, M., Foster, D. J., & Pfeiffer, B. E. (2020). Alternating sequences of future and past behavior encoded within hippocampal theta oscillations. *Science, 370*(6513), 247-250. doi:10.1126/science.abb4151

Wikenheiser, A. M., & Redish, A. D. (2015). Hippocampal theta sequences reflect current goals. *Nature*

Neuroscience, 18(2), 289-294. doi:10.1038/nn.3909

Zhang, L., Lee, J., Rozell, C., & Singer, A. C. (2019). Sub-second dynamics of theta-gamma coupling in hippocampal CA1. *eLife, 8*, e44320. doi:10.7554/eLife.44320

Zheng, C., Bieri, K. W., Hsiao, Y. T., & Colgin, L. L. (2016). Spatial Sequence Coding Differs during Slow and Fast Gamma Rhythms in the Hippocampus. *Neuron, 89*(2), 398-408. doi:10.1016/j.neuron.2015.12.005

Zheng, C., Hwaun, E., Loza, C. A., & Colgin, L. L. (2021). Hippocampal place cell sequences differ during correct and error trials in a spatial memory task. *Nat Commun, 12*(1), 3373. doi:10.1038/s41467-021-23765-x

Zhu, N., Zhang, Y., Xiao, X., Wang, Y., Yang, J., Colgin, L. L., & Zheng, C. (2023). Hippocampal oscillatory dynamics in freely behaving rats during exploration of social and non-social stimuli. *Cognitive Neurodynamics, 17*(2), 411-429. doi:10.1007/s11571-022-09829-8

FIGURE LEGENDS

Fig.1 | The schematic of a model for theta sequence development

Fast gamma rhythms coordinate a subgroup of place cells which dominantly fires phase-locked to fast gamma (FG-cells). The development process of theta sequences is disrupted by excluding these FG-cells. A possible model would be that development of sweep-ahead structure of theta sequences is dependent on the slow gamma modulation, i.e. slow gamma phase precession, whereby spatial information could be highly compressed within theta cycles. FG-cells are those cells exhibiting slow gamma phase precession within theta cycles since from the early stage of sequence development, which occurs earlier than the cells not phase locked to fast gamma (NFG-cells).

Fig.2 | A subset of hippocampal place cells was modulated by fast gamma rhythms during exploration on a circular track.

(A) An example of simultaneously recorded LFPs (raw LFP, 65-100 Hz 25-45 Hz, bandpass filtered gamma rhythm) and spikes of place cells. (B) Firing characteristics of two examples of FG-cell and NFG-cell, including firing rate map, and phase modulation by fast and slow gamma during detected episodes. Spikes were represented by red lines on top of the gamma waveforms. MVL is short for mean vector length. (C) The normalized turning curve of place cells sorted by the center of mass of their main place field. The proportion of 4 types of cells identified according to different modulation by fast and slow gamma was shown on the right. (D) Mean vector length of FG-cells and NFG-cells across successive running laps (n=12 sessions from 4 rats). Data are presented as mean ± SEM. ***$p<0.001$.

Fig.3 | Theta sequences development was disrupted without FG-cells.

(A) Top, Example color-coded posterior probability distribution across time from a single lap. The running trajectory of the animal was indicated as white dashed line. Bottom, 4–12 Hz bandpass filtered theta rhythm. The beginning and end of theta sequences were indicated as red bars. (B) Examples of detected theta sequences decoded by 3 different decoders, all spikes from all cells (top, i.e. raw sequences), all spikes excluding those from FG-cells (middle, i.e. exFG-sequences) and all spikes excluding those from NFG-cells (bottom, i.e. exNFG-sequences). The white triangle indicates the animal's current position. (C) Weighted correlations between time and decoded positions among three types of sequences. (D) Averaged decoded probabilities by 3 types of decoders over 63 cm centered by the animal's current running position and 170 ms centered by the mid-time point of theta sequence for each lap, in a single recording session. (E) Weighted correlation of raw sequences was significantly increased with running laps (n=12 sessions). (F) The running speed did not change across laps. (G) The sweep-ahead structure of the exFG-sequences (red) was disrupted compared to that of exNFG-sequences (yellow). (H) The effect of excluding either FG-cells or NFG-cells on early (left) and late (right) development of theta sequences. Data are presented as mean ± SEM. *$p<0.05$, **$p<0.01$, ***$p<0.001$.

Fig.4 | Temporospatially compressed structure of theta sequences required a relatively large proportion of FG-cells.

(A) Examples of detected theta sequences in early development. Each column is a pair of theta sequences decoded by 2 different decoders, exFG-decoder (top, all spikes excluding those from FG-cells) and exNFG-decoder (bottom, all spikes

excluding those from NFG-cells), in a same theta cycle. The left 2 columns of sequences were detected from laps with a relatively small proportion (~10%) of FG-cells. The right 2 columns of sequences were detected from laps with a relatively large proportion (~35%) of FG-cells. W.Corr was short for weighted correlation of each sequence. (B) Same as (A), but for late development of theta sequences. (C) The difference of weighted correlation of sequences between exNFG-decoder and exFG-decoder in early development, as a function of the proportion of excluded cells. Each scatter represents data from each recording session. The dashed line is the linear regression line of all scatters. (D) Same as (C), but for late development of theta sequences. The difference of weighted correlation of sequences between exNFG-decoder and exFG-decoder in late development, was positively correlated with the proportion of excluded cells.

Fig.5 | FG-cells and NFG-cells exhibited similar firing characteristics.

(A) Spatial tuning curves of representative FG- and NFG-cells during exploration on the circular track. Each column of cells exhibited similar place field positions on the track. (B) Distribution of the place field centers of mass (COM) of FG-cells and NFG-cells as a function of position on the track. (C) Cumulative distribution of FG-cells and NFG-cells' place field COM. (D) Spike counts, (E) Mean firing rate in the place field, (F) Place field size, and (G) Spatial information FG-cells and NFG-cells. Data are presented as mean ± SEM.

Fig.6 | Slow gamma phase precession across successive gamma cycles occurred during late development of theta sequences.

(A) Probability distributions of slow gamma phases of spikes across successive slow gamma cycles within theta sequences. Gamma cycles within theta cycles were ordered, centered at cycle 0 (i.e., gamma cycle with maximal spiking). Slow gamma phases of spikes shifted systematically across successive slow gamma cycles. (B) Spikes' slow gamma phase did not significantly backward-shifted across successive slow gamma cycles during early development of theta sequences. (C) Same as (A), spikes' slow gamma phase significantly backward-shifted across successive slow gamma cycles during late development of theta sequences. The white dots denote the peak probability of the histogram.

Fig.7 | FG-cells constantly exhibited slow gamma phase precession across laps.

(A) Examples of slow gamma phase precession within theta cycles on single cell level. The top row shows posterior probability for theta sequences. The middle row shows the LFPs waveform in the same theta cycle of the theta sequence, with each slow gamma cycle divided by black lines. The bottom row shows the slow gamma phases of spikes from a representative cell activated in this theta cycle. The spikes occurred at earlier slow gamma phase in the late slow gamma cycles compared with those in the early slow gamma cycles. (B) The averaged slow gamma phase shift across N active cycles were significantly negative (N=2, 3 or $\geqslant$4). The red lines indicate the median and the black lines indicate the 25% and 75% quantile of group data. (C) Histogram of mean slow gamma phase shift averaged within each theta cycle of each lap. The histograms of the real data are shown in blue with blue triangle indicating median. The histograms of the mock data are shown in grey with black lines indicating the 95th confident interval of the their median. (D) The same

as (C) but for histogram of mean slow gamma phase shift averaged within each place cell of each lap. (E) Histogram of mean slow gamma phase shift averaged within each FG-cell (above x-axis) or NFG-cell (below x-axis) of each lap. The red and yellow triangles are the median of phase shift in FG-cells and NFG-cells respectively. *p<0.05, **p<0.01, ***p<0.001.

Fig.8 | The sweep-ahead structure of FG-cell sequences was positively correlated with the intensity of slow gamma phase precession during both early and late sequence development.

(A) Scatter plot of averaged slow gamma phase shift across slow gamma cycles within a theta cycle as a function of weighted correlation of all sequences during all laps. Left panel shows real data (blue) and right panel shows mock data by shuffling (gray). (B) Probability distributions of sequences falling in 4 quadrants (Q1-Q4) with slow gamma phase shift (<0 or >0) and weighted correlation (<0 or >0). (C) The count of sequences falling in Q1 (blue triangle) was significantly higher than 95% quantile of the shuffled data (black line). The gray histogram indicates the relative probability of mock data falling in Q1 by 1000 times shuffling. (D) Scatter plot of averaged slow gamma phase shift across slow gamma cycles within a theta cycle as a function of weighted correlation of FG-cell sequences during early development (top) and late development (bottom) of sequences. (E) Probability distributions of FG-cell sequences falling in 4 quadrants during early development (top) and late development (bottom) of sequences. (F) The count of FG-cell sequences falling in Q1 (red triangle) was significantly higher than 95% quantile of the shuffled data (black line) during both early development (top) and late development (bottom) of sequences. (G-H) Same as (D-E), but for NFG-cell sequences. (I) The count of NFG-cell sequences falling in Q1 (red triangle) was significantly higher than 95% quantile of the shuffled data (black line) only during late (bottom) but not early (top) development of sequences. *p<0.05, ***p<0.001.

Figure 1

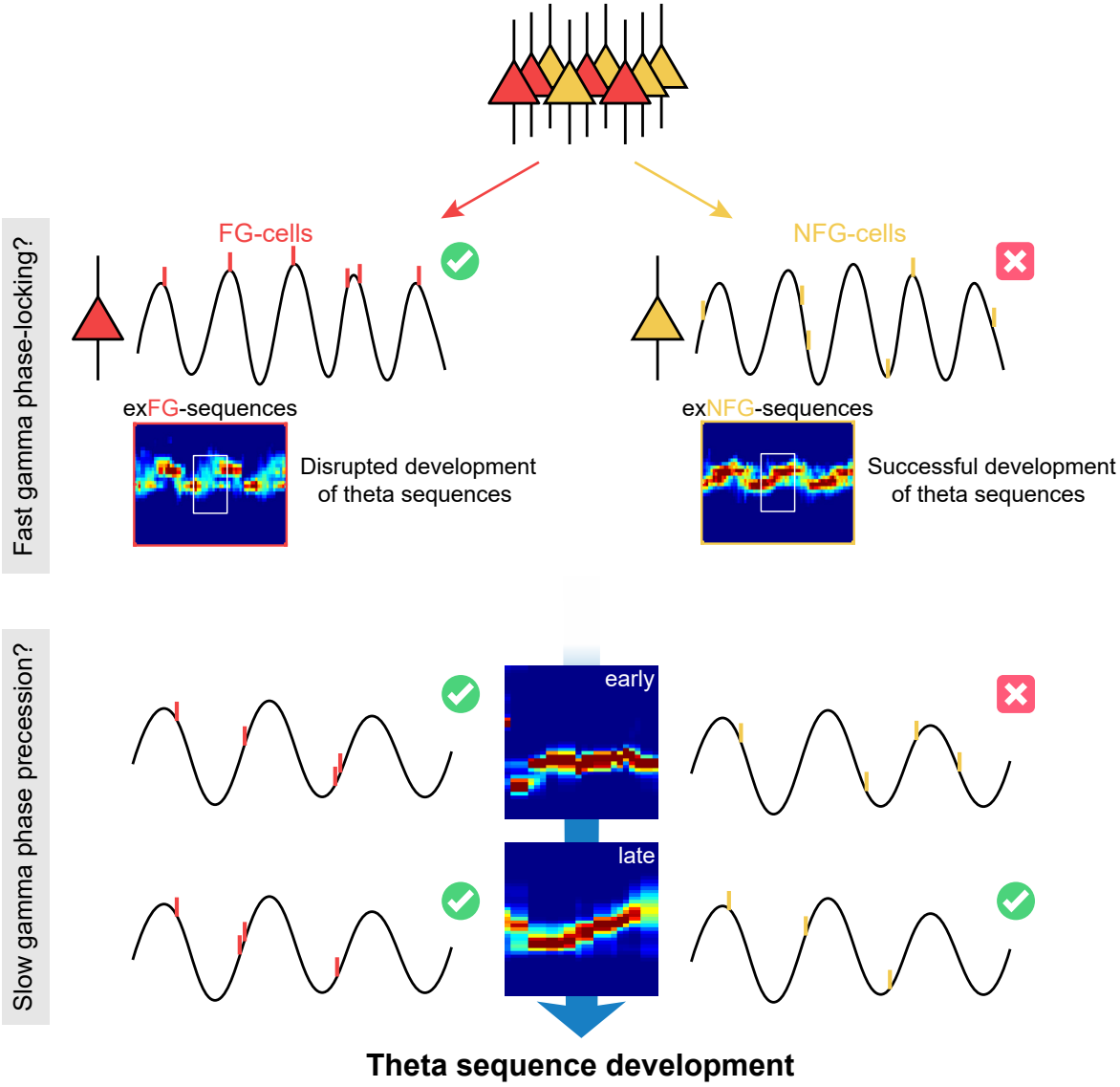
Fast gamma phase-locking?
FG-cells
NFG-cells
exFG-sequences
Disrupted development of theta sequences
exNFG-sequences
Successful development of theta sequences
Slow gamma phase precession?
early
late
Theta sequence development

Figure 2

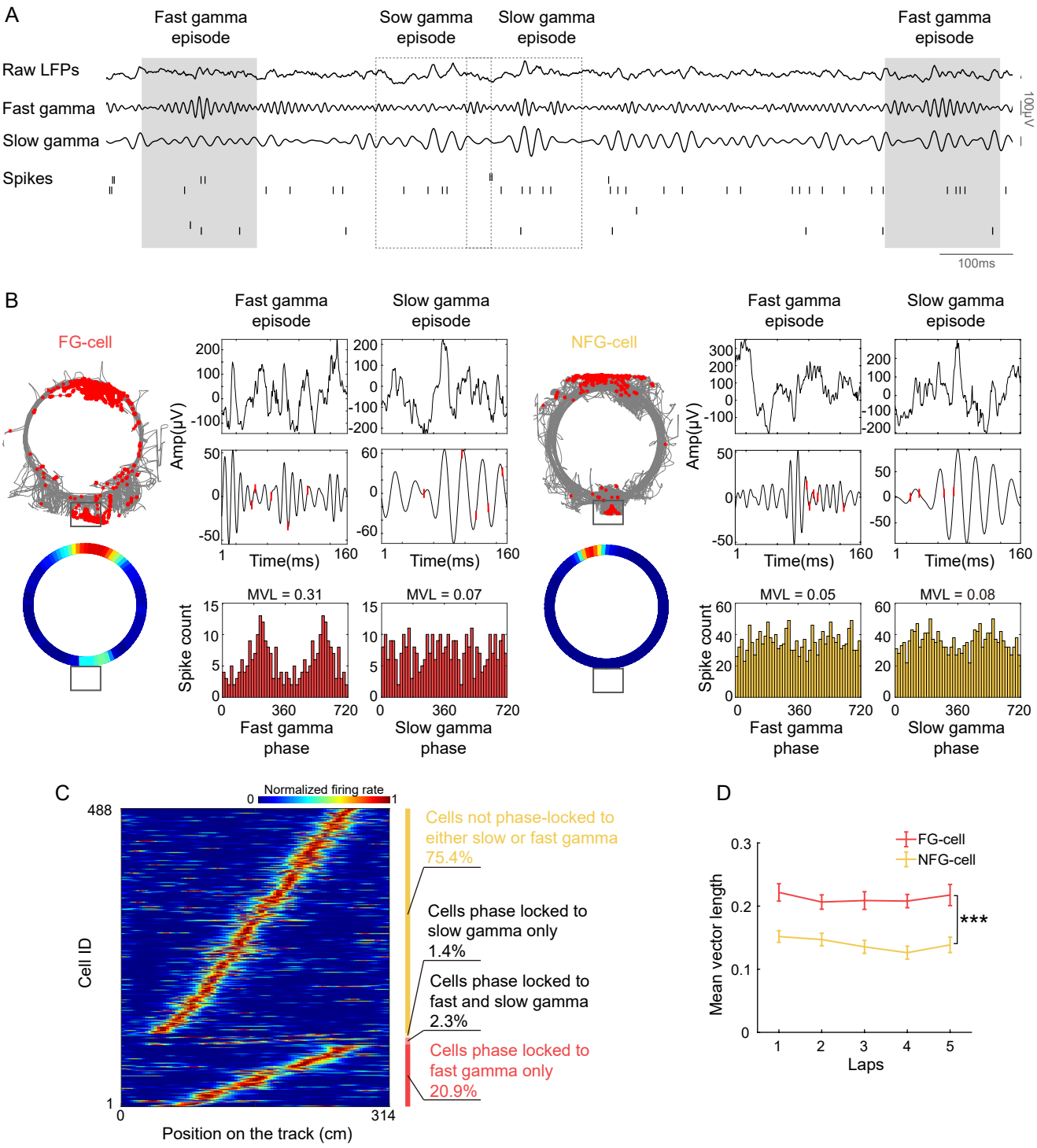
A
Fast gamma episode
Sow gamma episode
Slow gamma episode
Fast gamma episode
Raw LFPs
Fast gamma
Slow gamma
Spikes
100μV
100ms
B
FG-cell
NFG-cell
Fast gamma episode
Slow gamma episode
Amp(μV)
Time(ms)
Spike count
MVL = 0.31
MVL = 0.07
MVL = 0.05
MVL = 0.08
Fast gamma phase
Slow gamma phase
C
Normalized firing rate
Cell ID
Position on the track (cm)
Cells not phase-locked to either slow or fast gamma 75.4%
Cells phase locked to slow gamma only 1.4%
Cells phase locked to fast and slow gamma 2.3%
Cells phase locked to fast gamma only 20.9%
D
FG-cell
NFG-cell
Mean vector length
Laps
***

Figure 3

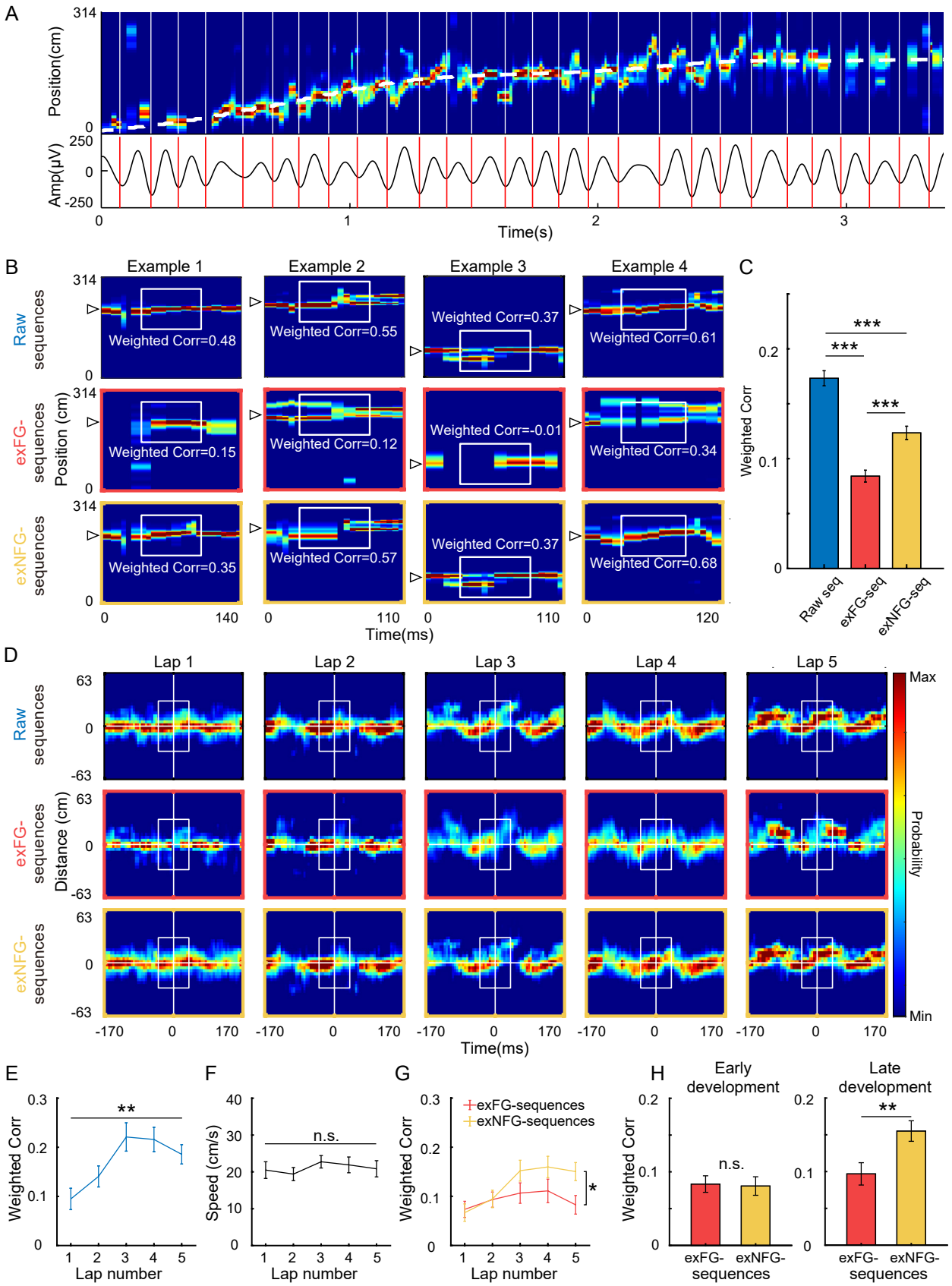
A
Position(cm)
Amp(μV)
Time(s)
B
Example 1
Example 2
Example 3
Example 4
Raw sequences
exFG-sequences
exNFG-sequences
Position (cm)
Weighted Corr=0.48
Weighted Corr=0.55
Weighted Corr=0.37
Weighted Corr=0.61
Weighted Corr=0.15
Weighted Corr=0.12
Weighted Corr=-0.01
Weighted Corr=0.34
Weighted Corr=0.35
Weighted Corr=0.57
Weighted Corr=0.37
Weighted Corr=0.68
Time(ms)
C
Weighted Corr
Raw seq
exFG-seq
exNFG-seq
D
Lap 1
Lap 2
Lap 3
Lap 4
Lap 5
Distance (cm)
Max
Min
Probability
Time(ms)
E
Weighted Corr
Lap number
F
Speed (cm/s)
n.s.
Lap number
G
exFG-sequences
exNFG-sequences
Weighted Corr
Lap number
H
Early development
Late development
Weighted Corr
n.s.
exFG-sequences
exNFG-sequences

Figure 4

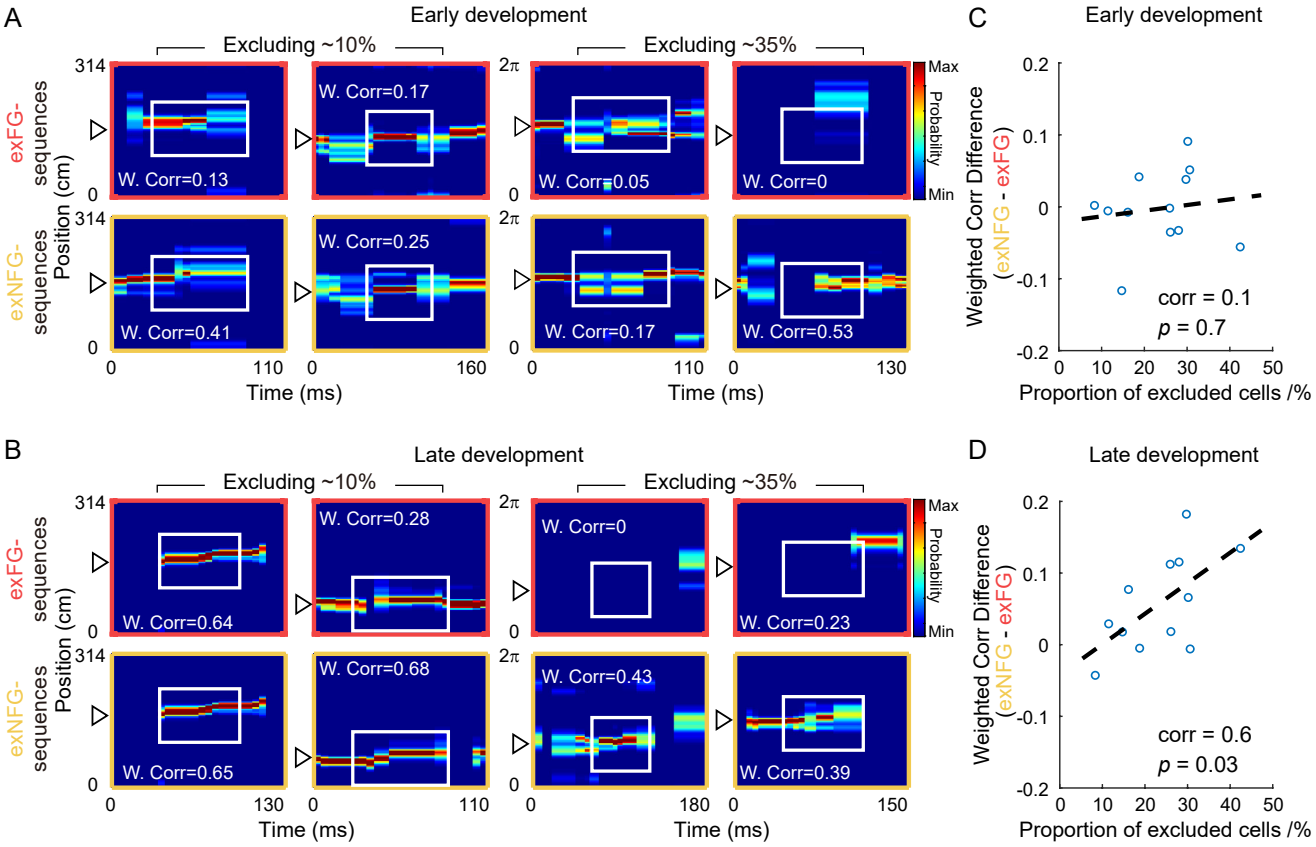
A
Early development
Excluding ~10%
Excluding ~35%
exFG-sequences
exNFG-sequences
Position (cm)
314
0
2π
W. Corr=0.13
W. Corr=0.17
W. Corr=0.05
W. Corr=0
W. Corr=0.41
W. Corr=0.25
W. Corr=0.17
W. Corr=0.53
Max
Probability
Min
0
110
160
130
Time (ms)
B
Late development
W. Corr=0.64
W. Corr=0.28
W. Corr=0
W. Corr=0.23
W. Corr=0.65
W. Corr=0.68
W. Corr=0.43
W. Corr=0.39
180
150
C
Weighted Corr Difference
(exNFG - exFG)
0.2
0.1
-0.1
-0.2
corr = 0.1
p = 0.7
10
20
30
40
50
Proportion of excluded cells /%
D
corr = 0.6
p = 0.03

Figure 5

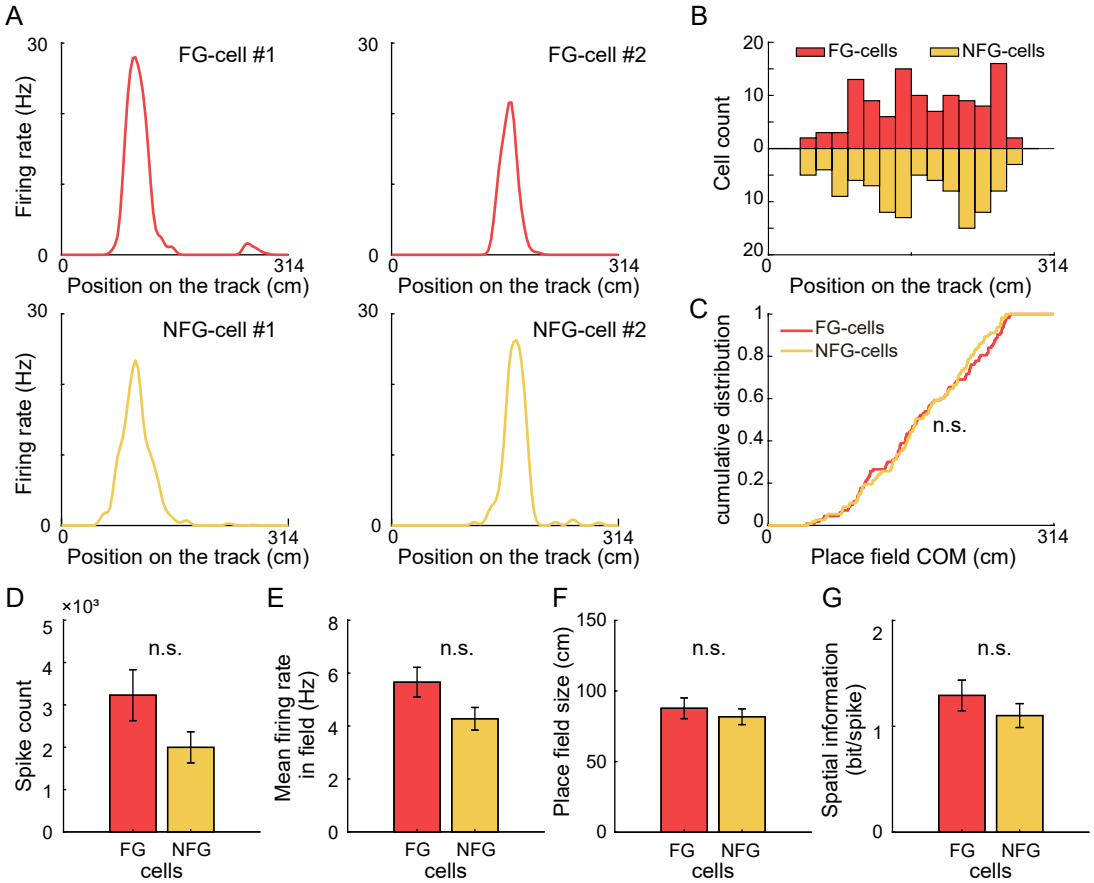
A
FG-cell #1
FG-cell #2
NFG-cell #1
NFG-cell #2
Firing rate (Hz)
Position on the track (cm)
B
FG-cells
NFG-cells
Cell count
C
cumulative distribution
n.s.
Place field COM (cm)
D
×10³
Spike count
E
Mean firing rate in field (Hz)
F
Place field size (cm)
G
Spatial information (bit/spike)
n.s.
FG
NFG
cells

Figure 6

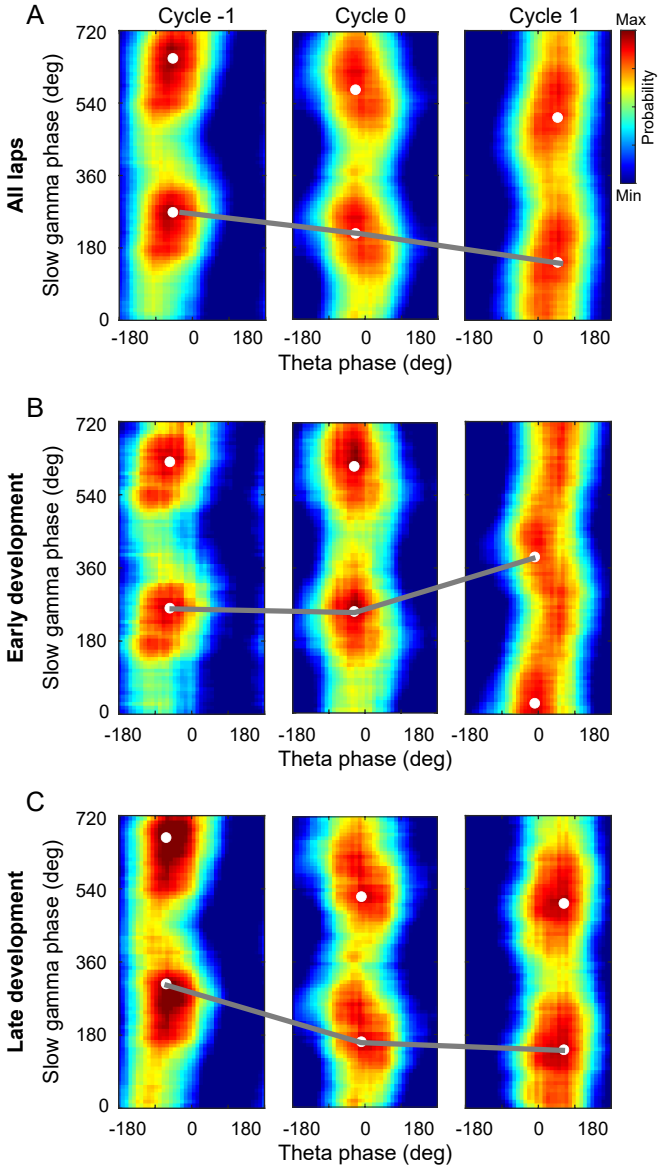
A
Cycle -1
Cycle 0
Cycle 1
Max
Probability
Min
All laps
Slow gamma phase (deg)
720
540
360
180
0
-180
0
180
Theta phase (deg)
B
Early development
C
Late development

Figure 7

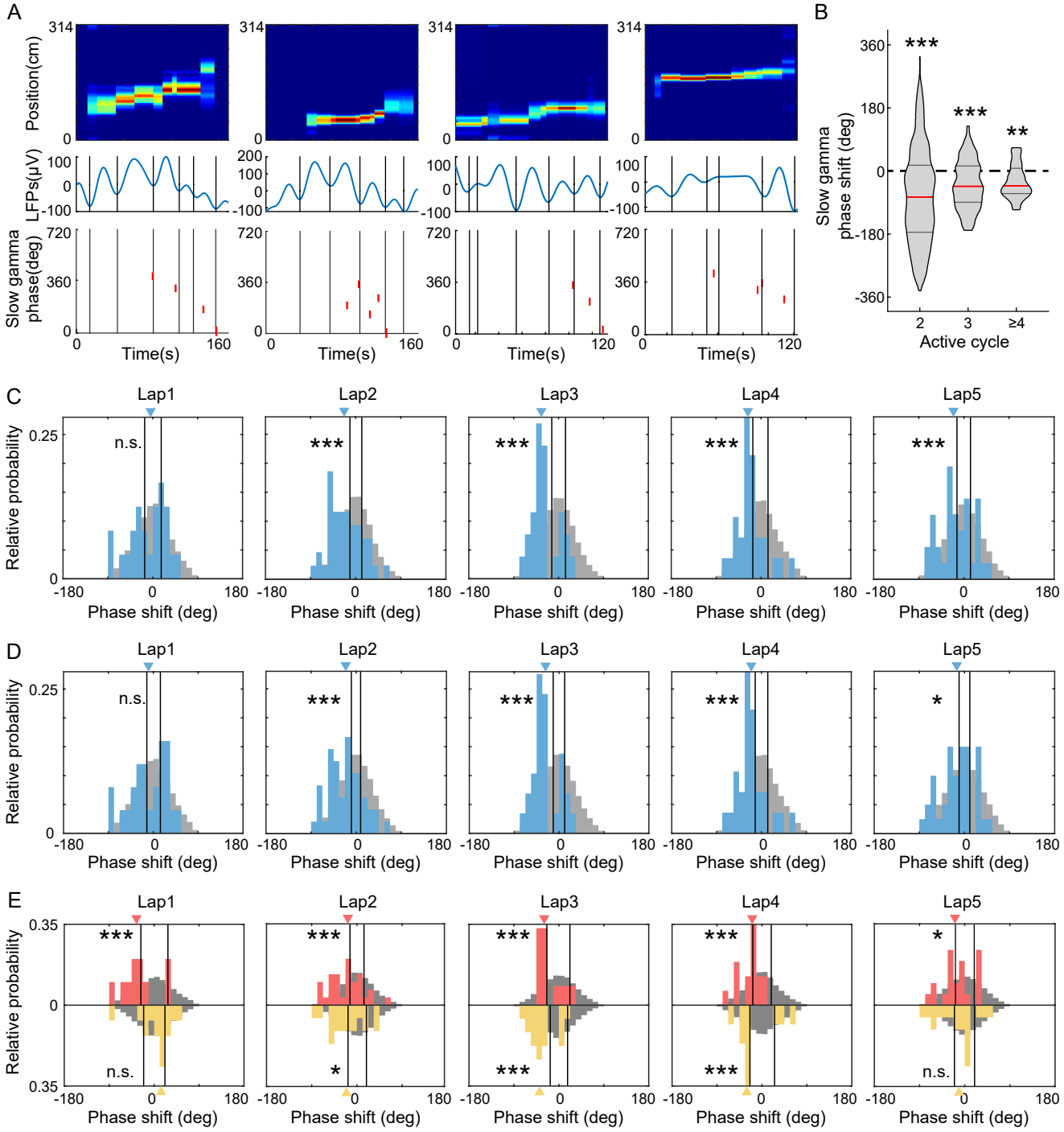
A
Position(cm)
LFPs(μV)
Slow gamma phase(deg)
Time(s)
B
Slow gamma phase shift (deg)
Active cycle
C
D
E
Lap1
Lap2
Lap3
Lap4
Lap5
Relative probability
Phase shift (deg)
n.s.
***
**
*

Figure 8

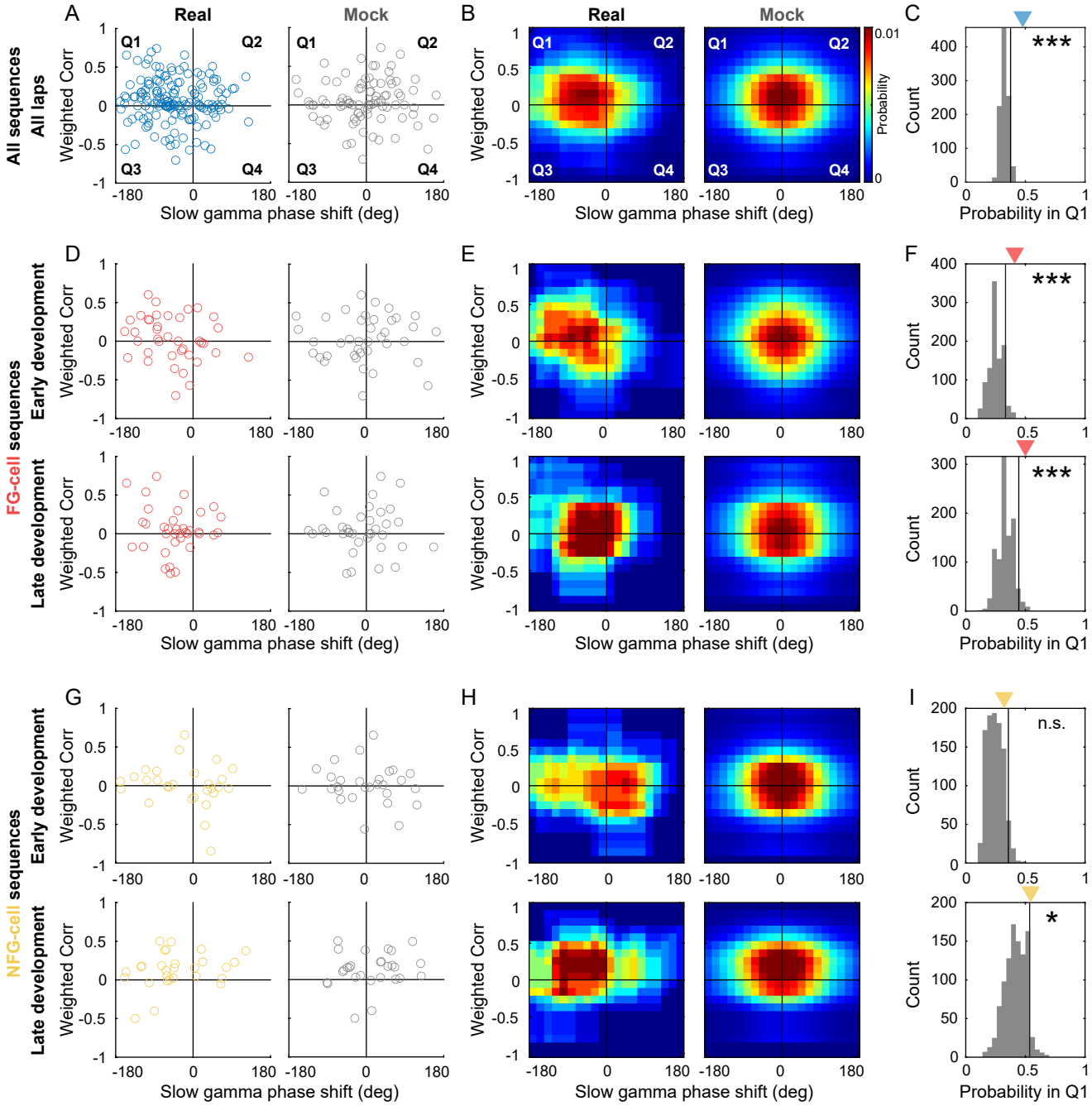
A
Real
Mock
B
Real
Mock
C
All sequences
All laps
FG-cell sequences
Early development
Late development
NFG-cell sequences
Early development
Late development
Q1
Q2
Q3
Q4
Weighted Corr
Slow gamma phase shift (deg)
Probability
0.01
0
Count
Probability in Q1
***
n.s.
*